Butyrate improves cardiac function and sympathetic neural remodeling following myocardial infarction in rats

Title: Butyrate improves cardiac function and neural remodeling

Xiaojie Jiang, Xin Huang, Yifan Tong, Hong Gao *

Department of Cardiology, The First Hospital of Nanchang， The Third Affiliated Hospital Of Nanchang University. Xiangshan North Road 128，Nanchang, 330008，Jiangxi, China.

*Corresponding Author: Hong Gao, E-mail: jiangxiaojie816@163.com.

Abstract

Increased inflammation is found in the cardiac sympathetic neural remodeling with malignant ventricular arrhythmia (VA) following myocardial infarction (MI). Butyrate, as a microbiota-derived short-chain fatty acids, can inhibit inflammation and myocardial hypertrophy. However, the role of butyrate in sympathetic neural remodeling after MI is unknown. This study aimed to investigate whether butyrate could improve cardiac dysfunction and VA following MI by regulating inflammation and sympathetic neural remodeling. MI rats were randomized to administrate the butyrate or vehicle through intraperitoneal injection to undergo the study. Our data demonstrated that butyrate treatment preserved the partial cardiac function at the 7 days post-MI. Butyrate downregulated the expression of essential for inflammatory response in the infarct border zone at the 3 days post-MI. Particularly, Butyrate promoted expression of M2 macrophage markers. Increased expressions of nerve growth factor (NGF) and norephinephrine (NE) at the 7 days after MI were inhibited in butyrate-treated rats. Furthermore, Butyrate significantly decreased the density of nerve fibers for growth-associated protein-43 (GAP-43) and tyrosine hydroxylase (TH) and resulted in less episodes of inducible VA. In conclusion, butyrate administration ameliorated cardiac function and VA after MI possibly through promoting M2 macrophages polarization to suppress inflammatory responses and inhibiting sympathetic neural remodeling, and may present an effectively pharmacological strategy for the prevention of MI-related remodeling.

Keywords: butyrate, myocardial infarction, ventricular arrhythmias, macrophage polarization, sympathetic neural remodeling.

Introduction

Myocardial infarction (MI) is associated with an increased risk of cardiovascular morbidity and mortality, a unique disease that can progress towards overt heart failure (HF) and malignant ventricular arrhythmia (VA) (Solomon et al. 2005). Previous studies have indicated that heterogeneous cardiac nerve sprouting and sympathetic hyperinnervation, also known as sympathetic neural remodeling, contribute to the development of HF and lethal VA in both patients and animal models of MI (Chen et al. 2010; Colucci et al. 2000; Zhou et al. 2004).

Growing evidences demonstrated that inflammatory responses are involved in the pathogenesis of MI-related VA via affecting cardiac remodeling, including structural, electrical and neural remodeling (Suthahar et al. 2017; Zarrouk-Mahjoub et al. 2016). Therein, macrophages act as pivotal role in mediating post-MI cardiac remodeling. Interestingly, promoting the transition of pro-inflammatory M1 macrophages to anti-inflammatory M2 macrophages can improve these adverse consequences. Timely regulation of M2/M1 ratio in the infarct border zone (IBZ) should be conducive to the prevention of inflammation, promote wound healing and inhibit cardiac fibrosis after MI (Cheng and Rong 2018), and can also ameliorate cardiac sympathetic nerve remodeling by reducing the secretion of nerve growth factor (NGF) and density of growth-associated protein-43 (GAP-43) and tyrosine hydroxylase (TH) during the infarct repair processes (Hu et al. 2019; Yang et al. 2016; Yin et al. 2016).

Butyrate, a short-chain fatty acids (SCFAs), derives from an intestinal microbial metabolism by resolving undigested resistant starches and dietary fibers (Mollica et al. 2017). Many studies have previously estimated butyrate cardioprotective effects of butyrate and derivative phenylalanine-butyramide in some animal models. For instance, butyramide can protect from doxorubicin-induced cardiotoxicity by limiting oxidative stress injury (Russo et al. 2019), and butyrate can protect against high-fat diet-induced cardiac tissue damage through improving cardiometabolic disorders and antioxidant defenses and partial abdominal aorta constriction (PAAC)-induced cardiac hypertrophy (Badejogbin et al. 2019; Patel 2018). Meanwhile, Butyrate

can attenuate lung and intestinal inflammation (Simeoli et al. 2017; Vieira et al. 2019). Furthermore, butyramide was once thought to have antiarrhythmic potential (Yen et al. 1974), however, the underlying mechanisms are still extremely understood.

On the basis of all its characteristics, therefore, in this study, we aimed at evaluating whether MI-induced cardiac dysfunction and VA can be reversed by intraperitoneal treatment of butyrate, whether these changes were mediated by reducing cardiac inflammation and sympathetic neural remodeling.

Materials and methods

Animal care

All male Sprague-Dawley rats (8-10 weeks age) were obtained from the Hubei provincial center for disease control and prevention (Hubei Province, China). All animals were housed under constant climatic conditions with free access to standard rodent chow and water. All experimental procedures were performed in accordance with ethical standards as formulated in the National Institutes of Health Guide for the Care and Use of Laboratory Animals (NIH, revised in 1996).

MI model and drug intervention

MI model was created by ligating the left anterior descending coronary artery according to previous method (Wang et al. 2016). MI rats were assigned by random numbers and double-blind operation to be intraperitoneally injected (i.p.) with either the 1 mol/L butyrate (butyric acid, 7.5 ml/kg) (Sigma-Aldrich, St. Louis, MO, USA) diluted in phosphate-buffered saline (PBS) or equal volume PBS immediately after MI surgery (Vieira et al. 2019). Sham-operated rats without ligation also received PBS. All drugs were given once a day consecutively until rats were euthanized or sacrificed at 3 or 7 days post-MI. The rats were sacrificed by intravenous injection of 2 mol/l KCl after anesthesia. All the tested specimens were collected from the infarct border zone (IBZ, < 2 mm outside the infarct).

Echocardiography and Hemodynamic Parameters

Transthoracic echocardiography was performed by an ultrasound machine (Visual Sonics Inc., Toronto, Canada) with a 716 probe used to quantify left ventricular end-diastolic (LVEDD),

ejection fraction (EF) and fractional shortening (FS) on 7 days post-MI. Anesthesia was induced via inhalation of 2% isoflurane gas in an induction box, and then fastened in the supine position on a heating board to maintain normothermia. These echocardiographs were operated by the same detector who was blinded to the experimental groups. Measurements were obtained from the LV parasternal long axis (B-mode) and short axis (M-mode) views. LV end diastolic volume (LVEDV) and LV end systolic volume (LVESV) from B-mode was ascertained using Simpson's method of disks and used to calculate EF. EF is calculated by (LVEDV-LVESV) / LVEDV×100%. FS was measured as % FS = (LVEDD- LVESD) / LVEDD×100% (LV end-systolic diameter, LVESD), LVEDD and LVESD was acquired from M-mode tracings. All measurements were averaged over three consecutive cardiac cycles.

After euthanized, the right carotid artery was imbedded with pressure transducer catheter (SPR-320, Millar, Inc., Houston, USA) filled with heparinized saline solution and then advanced into the LV. Hemodynamic data, including maximal rate of LV pressure rise and fall ($dP/dt_{max/min}$) were continuously recorded and analyzed using a LabChart 7 Pro (AD Instruments, Australia).

Immunohistochemistry

Infarct size was evaluated by staining with Masson's trichrome. After the heart tissues were embedded in paraffin, Masson's trichrome staining was executed 5 μm paraffin sections. The infarcted area was presented as the percentage of stained fibrosis area over total LV using the Image-Pro Plus software.

For Immunofluorescence, hearts were perfused with 10% formalin for fixation. After dehydrated and paraffin embedded, the sections were taken at 5 μm, and then permeabilized, blocked and incubated overnight with the primary anti-CD68 antibody (1:200; Abcam, Cambridge, UK), anti-CD163 (1/1,000; Abcam), anti-NGF (1:1000; Santa Cruz Biotechnology, Santa Cruz, CA, USA), anti-TH (1:500; Abcam) and anti-GAP43 (1:200; Abcam). Nuclei were counterstained with 4'-6-diamidino-2-phenylindole (DAPI; 1:2000; Millipore, Beverly, MA, USA). Images were obtained at 400× magnification with a fluorescence microscope ((IX-71; Olympus, Tokyo, Japan). Data were quantified by Image-Pro Plus software 6.0.

Enzyme-linked immunosorbent assay (ELISA)

The concentration of brain natriuretic peptide (BNP), Tumor Necrosis Factor (TNF)-α, interleukin (IL)-1β, IL-10 and norephinephrine (NE) from plasma or tissues were evaluated using commercial ELISA kits according to the instruction manual (BD Biosciences, San Jose, CA). Tissue ELISA measurements were normalized to the protein content of the homogenates.

Real-time reverse transcription-PCR (RT-PCR)

Total RNA from tissues was extracted with Trizol reagent (Invitrogen, Carlsbad, CA, USA). After quantification, cDNA was synthesized using a PrimeScript RT reagent Kit (Takara, Otsu, Japan). mRNA expression of target genes was analyzed by RT-PCR using fluorescent SYBR Green (Prism 7300, Applied Biosystems). The relative quantity of mRNAs was standardized with GAPDH as reference control. PCR primers used for mRNA quantitation are showed as following: (5'-3'): TNF-α forward: GTGATCGGTCCCAACAAGGA and reversed: AAGGTACCGGGTCTGGGA; IL-1β forward: GGAAGGCAGTGTCACTCATTGTG and reversed: GGT CCT CAT CCT GGA AGCTCC; IL-10 forward: TGCCTTCAGTCAAGTGAAGAC and reversed: AAACTCATTCAT-GGCCTTGTA; CD68 forward: ACCCGGAGACGACAATCAAC and reversed: CTTGGTGGCCTACAGAGTGG; CD163 forward: AGCTAGGATGCCCAACTTTGAT and reversed: TCTTCCTGAGCATCGGTTGTC; NGF forward: TCCACCCACCCAGTCTTCCA and reversed: GCCTTCCTGCTGAGCACACA; GAPDH forward: TTCAATGGCACAGTCAAGGC and reversed: TCACCCCATTTGATGTTAGCG.

Western blot

Protein were obtained from homogenized tissues and extracted in lysis buffer containing protease inhibitors, and then protein (50μg) was separated by 10% SDS-PAGE and transferred to a PVDF membrane using the electrophoretic method. The membrane was subsequently blocked and incubated with primary antibody against TH (1:500; Abcam), GAP43 (1:200; Abcam) and GAPDH (1:2,000, CST, Beverly, MA, USA). Following these, the membrane were incubated with a horseradish peroxidase (HRP)-conjugated secondary antibody (1:10,000; Aspen Biotechnology, Bedford, MA, USA). Proteins were detected using an ECL detection kit. The relative protein band intensity was analyzed and quantified using the Image J software and normalized to the GAPDH

level.

Electrocardiographic recordings

Surface ECG was monitored using AD Instruments for each animal anaesthetized by a 2% isoflurane oxygen mixture with subcutaneous electrodes placed in lead II position. An ECG sample of 30 min of every animal was analyzed. Time intervals, including P wave duration, PR interval and QJ interval, were measured with LabChart7 analysis software (Xue et al. 2019).

Inducibility of ventricular arrhythmias

Langendorff-perfused hearts were prepared according to previous methods (Chen et al. 2017; Shuai et al. 2019). In brief, after injected heparin sodium and anesthetized. Isolated perfused hearts were suspended on Langendorff apparatus (AD Instruments, Australia) with perfusion of HEPES-buffered Tyrode's solution (mM: NaCl 130, KCl 5.4, $CaCl_2$ 1.8, Na_2HPO_4 0.3, $MgCl_2$ 1, HEPES 10, glucose 10; pH adjusted to 7.35 with NaOH) at a constant pressure of 60 mm Hg to evaluate the VA inducibility. Recording should be started after stabilization for 20 min. Teflon-coated Ag-AgCl bipolar electrodes as a stimuli were placed on the right ventricle (RV), recordings were acquired at the LV. The induction of VA, including ventricular tachycardia (VT) and ventricular fibrillation (VF), was tested by applying burst pacing (2 ms pulses at 50 Hz, 1 s burst duration, interval 30s) for 3 minute.

Statistical analysis

Continuous data are expressed as means ± SD. Statistical analysis was performed with the SPSS statistical software 22.0 and GraphPad Prism 6.0. Differences among the groups of rats were tested with an ANOVA by a Tukey's test. Incidence of arrhythmias was compared by Fisher's exact test. $P < 0.05$ was considered to be significant.

Results

Butyrate suppresses cardiac dysfunction following MI

Improving the inflammatory response after MI can enhance cardiac function, and combined with the known anti-inflammatory and cardioprotective effects of butyrate in the different models, we

evaluated the effect of butyrate on cardiac function in the early stage of MI. The MI groups after 7 days showed a significant expansion in LVEDD and reduction in EF and FS, whereas treatment of butyrate significantly reversed these adverse changes (Figures 1 A-C). Accordingly, hemodynamic measurements, including dP/dtmax and dP/dtmin, displayed notable reduction and the serum levels of BNP simultaneously upregulated in MI groups compared with sham groups, butyrate-treated MI rats achieved greater dP/dtmax and dP/dtmin and less BNP levels (Figures 1 D-F). As expected, MI resulted in incremental heart weight/body weight (HW/BW) and lung weight/body weight (LW/BW) ratios, which might be related to water and sodium retention and reduced activity in rats with HF after MI, these indexes were significantly downregulated in butyrate-treated MI groups (Table 1). Moreover, butyrate also reduced infarct size of hearts after MI in rats (Table 1). These results revealed that butyrate increased LV contraction and decreased the HF degree in MI-induced rats.

Butyrate has the potential to prevent ventricular tachyarrhythmia following MI

The potentially arrhythmogenic substrate have been established within the first week post-MI (Penela et al. 2017). Meanwhile, the changes of cardiac function and neural remodeling on the 7 day after MI are probably the adjacent performance by affecting the production of M2 macrophages on the 3 day (Jung et al. 2017; Yin et al. 2016). However, the occurrence of arrhythmia is related to cardiac dysfunction and neural remodeling after MI. Taking into account the above reasons, we further evaluate the occurrence of VA by butyrate intervention at day 7 after MI. We observed basic electrical properties in vivo and found that MI rats at day 7 after MI operation presented remarkably prolongations in P wave duration and QJ intervals, and not significantly changed PR intervals. Treatment with butyrate following MI was able to significantly shorten P wave duration, wave duration and QJ intervals (Figures 2 A-D). In the isolated heart preparation, MI increased the incidence rate of malignant ventricular tachyarrhythmia (VT and VF), Treatment of MI rats with butyrate for 7 days after MI partially prevented VT/VF susceptibility (Figures 2 E, F). These data showed that butyrate treatment attenuated the vulnerability of lethal VA following MI.

Butyrate prevents cardiac inflammation by promoting M2 macrophages polarization post-MI

Due to the fact that Greatly promoting the M2 macrophages polarization at day 3 can significantly improve the degree of short-term (day 3 or 7) inflammation after MI (Jung et al. 2017; Kimbrough et al. 2018; Shirakawa et al. 2018), we studied the effect of butyrate on promotion of M2 macrophages polarization at day 3 after MI. Compared with sham-treated rats, all rats exhibited significant pro-inflammatory response at day 3 in post-MI induction, as we had observed, upregulated pro-inflammatory cytokines TNF-α and IL-1βwere detected by RT-PCR and Elisa analysis in the IBZ, no significant difference was observed in the anti-inflammatory cytokine IL-10 of MI groups . However, Administration of butyrate inhibited the expression of the TNF-α and IL-1βand promoted the production of IL-10 post-MI (Figures 3 A-F). Additionally, immunofluorescence analysis showed that CD68-positive ($CD68^+$) cells were massive located in the border areas of infarcted hearts compared with sham groups, no difference of $CD163^+/CD68^+$ macrophages was observed between the sham groups and MI groups at this time point. $CD68^+$ macrophages were rarely observed in butyrate-treated MI rats, conversely, butyrate significantly increased the infiltration of $CD163^+/CD68^+$ macrophages (Figures 3 G-I). Similar results were verified by mRNA analysis of CD68 and CD163 (Figures 3 J, K). Our data demonstrated that butyrate inhibited inflammatory responses, at least in part, through the regulation of M2 macrophages polarization.

Butyrate inhibits MI-induced NGF and NE production

NGF-positive signals in cardiac macrophages ($NGF/CD68^+$ cells) in the peri-infarcted area at day 7 post-MI were counted by immunofluorescence analysis. Significant increase in NGF-positive expression and $NGF/CD68^+$ cells was observed in the MI groups when compared to the control group, which was reduced in those rats that had received butyrate than those treated with vehicle (Figures 4 A-C). Similar Changes in NGF mRNA expression were also noted, although increased in the MI group, less in those who received butyrate (Figure 4 D). Moreover, we found that NE was markedly increased in the MI groups, butyrate treatment exhibited lower levels of NE in response to MI compared with those vehicle-treated MI rats of (Figures 4 E, F). These results suggested butyrate treatment efficiently reduced NGF expression by inhibiting macrophage activation.

Butyrate improves sympathetic neural remodeling

Considering that sympathetic hyperinnervation peaks at day 7 post-MI (Hasan et al. 2006; Zhou et al. 2004), we detected the markers of neurohyperplasia by using immunofluorescence and WB analysis. Evaluations of cardiac abnormal sympathetic innervation demonstrated that location of TH and GAP43-positive nerve fibers in the IBZ at 7 days post-MI were significantly increased in the MI groups compared to the sham groups, while butyrate markedly attenuated the expression of these markers (Figures 5 A-C). Similarly, MI displayed elevated cardiac TH and GAP43 protein expressions, we further confirmed the reduced capacity of butyrate in the elevation of TH and GAP43 expression after MI (Figures 5 D, E). The results indicated that continually administration of butyrate prevented cardiac sympathetic hyperinnervation and nerve sprouting by reducing TH and GAP43 expressions after MI.

Discussion

In this study, our study investigated an important information about the benefits of butyrate treatment on cardiac function and ventricular tachycardia (VTA) in MI rats and explored the possible mechanisms. Our data demonstrated that butyrate given to MI rats (1) improved cardiac function, (2) reduced electrical impulse conduction time and the incidence of VTA, (3) suppressed inflammatory responses probably through promoting M2 macrophages polarization, and (4) inhibited the release of NGF and NE, thereby to alleviate the sympathetic neural remodeling.

Recent studies have confirmed that promoting the transformation of M1 macrophages to M2 macrophages to inhibit inflammation is a new anti-inflammatory strategy. In addition, this transition of macrophage polarity can inhibit sympathetic nerve proliferation and sprouting after MI, and improve the progress of HF (Jung et al. 2017; Mongue-Din et al. 2017; Yang et al. 2016; Yin et al. 2016). According to the results of previous studies, it is suggested that promoting the transition of polarity of macrophages on the day 3 after MI is a critical time node to more efficiently inhibit inflammation (Bouhlel et al. 2007; Liu et al. 2014; Shirakawa et al. 2018). As expected, our studies showed that butyrate, which had anti-inflammatory effect, could also inhibit inflammation on the day 3 after MI probably by promoting the polarization of M2 macrophages. Furthermore, increased NGF derived from infiltrating macrophages following MI can cause sympathetic hyperinnervation (Hasan et al. 2006). On the contrary, reduction of NGF levels by

deleting macrophages and promoting M2 macrophages polarization can inhibit sympathetic hyperinnervation post-MI (Wernli et al. 2009; Yin et al. 2016). Meanwhile, previous studies verified an augmentation of NGF, which acted as an upregulated role in sympathetic hyperinnervation and mediated the immune and inflammatory responses following tissue injury, and NGF mRNA expression took 3 days to reach its peak in the border zone of the myocardial lesion (D'Elia et al. 2014; Nicol and Vasko 2007; Zhou et al. 2004), which suggested that regulating the polarity of macrophages at 3 days after MI may change the synthesis of NGF. Interestingly, in the present study, we also observed that butyrate reduces the generation of NGF post-MI possibly related to an excess of M2 macrophages at an earlier than expected time frame. Therefore, we could infer that this effect of promoting M2 macrophages polarization might be considered as a reason for butyrate to inhibit nerve remodeling and inflammation after MI. Cardiac nerve remodeling as a result of MI is known to be a major origin of lethal VTA. Heterogeneous sympathetic innervation may be beneficial in maintaining myocardial contraction for the time being, but can also result in deteriorated dispersion of repolarization and enhancive automaticity, triggers activity and initiation, which is underlying the vulnerability to malignant VA (Chen et al. 2010; Li and Li 2015). Consistent with previous findings, our results also showed that abundant expressions of TH and GAP43 in the early stage of MI, which respectively represented cardiac sympathetic hyperinnervation and nerve sprouting (Yin et al. 2016), were downregulated by butyrate treatment. Just as some drugs therapy, such as beta blocker, simvastatin and atorvastatin, have antiarrhythmic effect probably because they attenuates the arrhythmogenic effect of abnormal sympathetic hyperinnervation by reducing the production of TH and GAP43, which was chiefly associated with reduced inflammatory responses in the peri-infarcted area (Sun et al. 2017; Yang et al. 2016; Yu et al. 2012). We further investigated cardiac sympathetic function by detecting NE levels and found that butyrate implemented an ultimate effect.

Indeed, reducing the incidence of arrhythmia after MI is not only related to the attenuation of neural remodeling, but also to the improvement of worsening cardiac function and intra-ventricular conduction delay, in particular, inhibition of inflammatory responses after MI, these changes were conducive to improve substrate for malignant VA by decrease reentrant tachycardia and alter electrical remodeling, such as ion-channel expression or activity (De Jesus et

al. 2017; Francis Stuart et al. 2016; Parikh et al. 2019; Xue et al. 2019). Therefore, we cannot separate them from the beneficial targets. In the present study, we observed that butyrate treatment ameliorated cardiac dysfunction and QJ intervals. Correspondingly, we considered that attenuation of these factors from butyrate therapy can contribute to the anti-arrhythmia effects.

Our study has some limitations. First, since a significant amount of absorbed (via rumen) butyrate can be converted into ketones by orally administering, enteral administration may be a better choice. Second, we lack the results of butyrate concentration in plasma after administration. Third, Different doses of butyrate can more fully confirm the effect of butyrate on remodeling after MI.

Taken together, our results demonstrated that cardiac remodeling and inflammation, especially, the M1/M2 balance dysregulation and heterogeneous sympathetic innervation, were more pronounced in the presence of MI disease, and accompanied with a high incidence of malignant VA. Butyrate, as an anti-inflammatory substance, can facilitate macrophage phenotypic balance between M1 and M2 and regulate nerve remodeling, therefore be beneficial to improve the cardiac function and electrical stability, thereby to reduce arrhythmias. At the same time, we also know that butyrate is also a metabolite of intestinal flora. Combined with the observed results of our studies, we can infer that intestinal flora may also play a potential role in regulating cardiac remodeling after MI, which yet needs to be further confirmed.

Conflict of interest

The authors declare no potential conflicts of interest.

Authorship contributions

Xiaojie Jiang, designed the experiments and contributed to the writing of the manuscript; Hong Gao, designed the experiments and performed the data analysis; Xin Huang and Yifan Tong, conducted the experiments.

References

Badejogbin, C., Areola, D.E., Olaniyi, K.S., Adeyanju, O.A., and Adeosun, I.O. 2019. Sodium

butyrate recovers high-fat diet-fed female Wistar rats from glucose dysmetabolism and uric acid-associated cardiac tissue damage. Naunyn Schmiedebergs Arch Pharmacol. doi: 10.1007/s00210-019-01679-2.

Bouhlel, M.A., Derudas, B., Rigamonti, E., Dievart, R., Brozek, J., Haulon, S., Zawadzki, C., Jude, B., Torpier, G., Marx, N., Staels, B., and Chinetti-Gbaguidi, G. 2007. PPARgamma activation primes human monocytes into alternative M2 macrophages with anti-inflammatory properties. Cell Metab **6**(2): 137-143. doi: 10.1016/j.cmet.2007.06.010.

Chen, P.S., Choi, E.K., Zhou, S., Lin, S.F., and Chen, L.S. 2010. Cardiac neural remodeling and its role in arrhythmogenesis. Heart Rhythm **7**(10): 1512-1513. doi: 10.1016/j.hrthm.2010.05.020.

Chen, X., Qin, M., Jiang, W., Zhang, Y., and Liu, X. 2017. Electrophysiological characteristics of pressure overload-induced cardiac hypertrophy and its influence on ventricular arrhythmias. PLoS One **12**(9): e0183671. doi: 10.1371/journal.pone.0183671.

Cheng, Y.Y., and Rong, J.H. 2018. Macrophage Polarization as a Therapeutic Target in Myocardial Infarction. Current Drug Targets **19**(6): 651-662. doi: Pmid 29086692 10.2174/1389450118666171031115025.

Colucci, W.S., Sawyer, D.B., Singh, K., and Communal, C. 2000. Adrenergic overload and apoptosis in heart failure: Implications for therapy. Journal of Cardiac Failure **6**(2): 1-7.

D'Elia, E., Pascale, A., Marchesi, N., Ferrero, P., Senni, M., Govoni, S., Gronda, E., and Vanoli, E. 2014. Novel approaches to the post-myocardial infarction/heart failure neural remodeling. Heart Fail Rev **19**(5): 611-619. doi: 10.1007/s10741-013-9415-6.

De Jesus, N.M., Wang, L., Lai, J., Rigor, R.R., Francis Stuart, S.D., Bers, D.M., Lindsey, M.L., and Ripplinger, C.M. 2017. Antiarrhythmic effects of interleukin 1 inhibition after myocardial infarction. Heart Rhythm **14**(5): 727-736. doi: 10.1016/j.hrthm.2017.01.027.

Francis Stuart, S.D., De Jesus, N.M., Lindsey, M.L., and Ripplinger, C.M. 2016. The crossroads of inflammation, fibrosis, and arrhythmia following myocardial infarction. J Mol Cell Cardiol **91**: 114-122. doi: 10.1016/j.yjmcc.2015.12.024.

Hasan, W., Jama, A., Donohue, T., Wernli, G., Onyszchuk, G., Al-Hafez, B., Bilgen, M., and Smith, P.G. 2006. Sympathetic hyperinnervation and inflammatory cell NGF synthesis following myocardial infarction in rats. Brain Res **1124**(1): 142-154. doi: 10.1016/j.brainres.2006.09.054.

Hu, J., Huang, C.X., Rao, P.P., Zhou, J.P., Wang, X., Tang, L., Liu, M.X., and Zhang, G.G. 2019.

Inhibition of microRNA-155 attenuates sympathetic neural remodeling following myocardial infarction via reducing M1 macrophage polarization and inflammatory responses in mice. Eur J Pharmacol **851**: 122-132. doi: 10.1016/j.ejphar.2019.02.001.

Jung, M., Ma, Y., Iyer, R.P., DeLeon-Pennell, K.Y., Yabluchanskiy, A., Garrett, M.R., and Lindsey, M.L. 2017. IL-10 improves cardiac remodeling after myocardial infarction by stimulating M2 macrophage polarization and fibroblast activation. Basic Res Cardiol **112**(3): 33. doi: 10.1007/s00395-017-0622-5.

Kimbrough, D., Wang, S.H., Wright, L.H., Mani, S.K., Kasiganesan, H., LaRue, A.C., Cheng, Q., Nadig, S.N., Atkinson, C., and Menick, D.R. 2018. HDAC inhibition helps post-MI healing by modulating macrophage polarization. J Mol Cell Cardiol **119**: 51-63. doi: 10.1016/j.yjmcc.2018.04.011.

Li, C.Y., and Li, Y.G. 2015. Cardiac Sympathetic Nerve Sprouting and Susceptibility to Ventricular Arrhythmias after Myocardial Infarction. Cardiol Res Pract **2015**: 698368. doi: 10.1155/2015/698368.

Liu, Y.C., Zou, X.B., Chai, Y.F., and Yao, Y.M. 2014. Macrophage polarization in inflammatory diseases. Int J Biol Sci **10**(5): 520-529. doi: 10.7150/ijbs.8879.

Mollica, M.P., Raso, G.M., Cavaliere, G., Trinchese, G., De Filippo, C., Aceto, S., Prisco, M., Pirozzi, C., Di Guida, F., Lama, A., Crispino, M., Tronino, D., Di Vaio, P., Canani, R.B., Calignano, A., and Meli, R. 2017. Butyrate Regulates Liver Mitochondrial Function, Efficiency, and Dynamics in Insulin-Resistant Obese Mice. Diabetes **66**(5): 1405-1418. doi: 10.2337/db16-0924.

Mongue-Din, H., Patel, A.S., Looi, Y.H., Grieve, D.J., Anilkumar, N., Sirker, A., Dong, X., Brewer, A.C., Zhang, M., Smith, A., and Shah, A.M. 2017. NADPH Oxidase-4 Driven Cardiac Macrophage Polarization Protects Against Myocardial Infarction-Induced Remodeling. JACC Basic Transl Sci **2**(6): 688-698. doi: 10.1016/j.jacbts.2017.06.006.

Nicol, G.D., and Vasko, M.R. 2007. Unraveling the story of NGF-mediated sensitization of nociceptive sensory neurons: ON or OFF the Trks? Mol Interv **7**(1): 26-41. doi: 10.1124/mi.7.1.6.

Parikh, M., Raj, P., Austria, J.A., Yu, L., Garg, B., Netticadan, T., and Pierce, G.N. 2019. Dietary flaxseed protects against ventricular arrhythmias and left ventricular dilation after a myocardial infarction. J Nutr Biochem **71**: 63-71. doi: 10.1016/j.jnutbio.2019.06.004.

Patel, B.M. 2018. Sodium Butyrate Controls Cardiac Hypertrophy in Experimental Models of Rats. Cardiovasc Toxicol **18**(1): 1-8. doi: 10.1007/s12012-017-9406-2.

Penela, D., Acosta, J., Andreu, D., Ortiz-Perez, J.T., Bosch, X., Perea, R.J., de Caralt, T.M., Fernandez-Armenta, J., Soto-Iglesias, D., Prat-Gonzalez, S., Borras, R., Mont, L., Hervas, V., Morales-Ruiz, M., Jimenez, W., Mira, A., Donnelly, J., Ekinci, O., Lasalvia, L., and Berruezo, A. 2017. Identification of the potentially arrhythmogenic substrate in the acute phase of ST-segment elevation myocardial infarction. Heart Rhythm **14**(4): 592-598. doi: 10.1016/j.hrthm.2017.01.019.

Russo, M., Guida, F., Paparo, L., Trinchese, G., Aitoro, R., Avagliano, C., Fiordelisi, A., Napolitano, F., Mercurio, V., Sala, V., Li, M., Sorriento, D., Ciccarelli, M., Ghigo, A., Hirsch, E., Bianco, R., Iaccarino, G., Abete, P., Bonaduce, D., Calignano, A., Berni Canani, R., and Tocchetti, C.G. 2019. The novel butyrate derivative phenylalanine-butyramide protects from doxorubicin-induced cardiotoxicity. Eur J Heart Fail **21**(4): 519-528. doi: 10.1002/ejhf.1439.

Shirakawa, K., Endo, J., Kataoka, M., Katsumata, Y., Yoshida, N., Yamamoto, T., Isobe, S., Moriyama, H., Goto, S., Kitakata, H., Hiraide, T., Fukuda, K., and Sano, M. 2018. IL (Interleukin)-10-STAT3-Galectin-3 Axis Is Essential for Osteopontin-Producing Reparative Macrophage Polarization After Myocardial Infarction. Circulation **138**(18): 2021-2035. doi: 10.1161/Circulationaha.118.035047.

Shuai, W., Kong, B., Fu, H., Shen, C., and Huang, H. 2019. Loss of MD1 increases vulnerability to ventricular arrhythmia in diet-induced obesity mice via enhanced activation of the TLR4/MyD88/CaMKII signaling pathway. Nutr Metab Cardiovasc Dis **29**(9): 991-998. doi: 10.1016/j.numecd.2019.06.004.

Simeoli, R., Mattace Raso, G., Pirozzi, C., Lama, A., Santoro, A., Russo, R., Montero-Melendez, T., Berni Canani, R., Calignano, A., Perretti, M., and Meli, R. 2017. An orally administered butyrate-releasing derivative reduces neutrophil recruitment and inflammation in dextran sulphate sodium-induced murine colitis. Br J Pharmacol **174**(11): 1484-1496. doi: 10.1111/bph.13637.

Solomon, S.D., Zelenkofske, S., McMurray, J.J., Finn, P.V., Velazquez, E., Ertl, G., Harsanyi, A., Rouleau, J.L., Maggioni, A., Kober, L., White, H., Van de Werf, F., Pieper, K., Califf, R.M., Pfeffer, M.A., and Valsartan in Acute Myocardial Infarction Trial, I. 2005. Sudden death in patients with myocardial infarction and left ventricular dysfunction, heart failure, or both. N Engl J Med **352**(25): 2581-2588. doi: 10.1056/NEJMoa043938.

Sun, L., Yan, S., Wang, X., Zhao, S., Li, H., Wang, Y., Lu, S., Dong, X., Zhao, J., Yu, S., Li, M., and Li, Y. 2017. Metoprolol prevents chronic obstructive sleep apnea-induced atrial fibrillation by inhibiting structural, sympathetic nervous and metabolic remodeling of the atria. Sci Rep **7**(1): 14941. doi: 10.1038/s41598-017-14960-2.

Suthahar, N., Meijers, W.C., Sillje, H.H.W., and de Boer, R.A. 2017. From Inflammation to Fibrosis-Molecular and Cellular Mechanisms of Myocardial Tissue Remodelling and Perspectives on Differential Treatment Opportunities. Curr Heart Fail Rep **14**(4): 235-250. doi: 10.1007/s11897-017-0343-y.

Vieira, R.S., Castoldi, A., Basso, P.J., Hiyane, M.I., Camara, N.O.S., and Almeida, R.R. 2019. Butyrate Attenuates Lung Inflammation by Negatively Modulating Th9 Cells. Front Immunol **10**: 67. doi: 10.3389/fimmu.2019.00067.

Wang, D., Zhu, H., Yang, Q., and Sun, Y. 2016. Effects of relaxin on cardiac fibrosis, apoptosis, and tachyarrhythmia in rats with myocardial infarction. Biomed Pharmacother **84**: 348-355. doi: 10.1016/j.biopha.2016.09.054.

Wernli, G., Hasan, W., Bhattacherjee, A., van Rooijen, N., and Smith, P.G. 2009. Macrophage depletion suppresses sympathetic hyperinnervation following myocardial infarction. Basic Res Cardiol **104**(6): 681-693. doi: 10.1007/s00395-009-0033-3.

Xue, J., Yan, X., Yang, Y., Chen, M., Wu, L., Gou, Z., Sun, Z., Talabieke, S., Zheng, Y., and Luo, D. 2019. Connexin 43 dephosphorylation contributes to arrhythmias and cardiomyocyte apoptosis in ischemia/reperfusion hearts. Basic Res Cardiol **114**(5): 40. doi: 10.1007/s00395-019-0748-8.

Yang, N., Cheng, W., Hu, H., Xue, M., Li, X., Wang, Y., Xuan, Y., Li, X., Yin, J., Shi, Y., and Yan, S. 2016. Atorvastatin attenuates sympathetic hyperinnervation together with the augmentation of M2 macrophages in rats postmyocardial infarction. Cardiovasc Ther **34**(4): 234-244. doi: 10.1111/1755-5922.12193.

Yen, C.H., Lowrie, H.S., and Dean, R.R. 1974. Compounds related to 4-disopropylamino-2-phenyl-2(2-pyridyl)butyramide. Their synthesis and antiarrhythmic activity. J Med Chem **17**(11): 1131-1135. doi: 10.1021/jm00257a001.

Yin, J., Hu, H., Li, X., Xue, M., Cheng, W., Wang, Y., Xuan, Y., Li, X., Yang, N., Shi, Y., and Yan, S. 2016. Inhibition of Notch signaling pathway attenuates sympathetic hyperinnervation together with the augmentation of M2 macrophages in rats post-myocardial infarction. Am J

Physiol Cell Physiol **310**(1): C41-53. doi: 10.1152/ajpcell.00163.2015.

Yu, T., Zhu, W., Gu, B., Li, S., Wang, F., Liu, M., Wei, M., and Li, J. 2012. Simvastatin attenuates sympathetic hyperinnervation to prevent atrial fibrillation during the postmyocardial infarction remodeling process. J Appl Physiol (1985) **113**(12): 1937-1944. doi: 10.1152/japplphysiol.00451.2012.

Zarrouk-Mahjoub, S., Zaghdoudi, M., Amira, Z., Chebi, H., Khabouchi, N., Finsterer, J., Mechmeche, R., and Ghazouani, E. 2016. Pro- and anti-inflammatory cytokines in post-infarction left ventricular remodeling. Int J Cardiol **221**: 632-636. doi: 10.1016/j.ijcard.2016.07.073.

Zhou, S., Chen, L.S., Miyauchi, Y., Miyauchi, M., Kar, S., Kangavari, S., Fishbein, M.C., Sharifi, B., and Chen, P.S. 2004. Mechanisms of cardiac nerve sprouting after myocardial infarction in dogs. Circ Res **95**(1): 76-83. doi: 10.1161/01.RES.0000133678.22968.e3.

Table 1. Effect of Butyrate on morphometric parameters and infarct size

	Sham (n=8)	MI (n=8)	Butyrate +MI(n=8)
BW (g)	227.6±5.3	240.0±5.7	231.1±5.2
HW (mg)	821.0±8.8	1057.0±45.4*	895.8±26.6$^{\#}$
HW/BW (mg/g)	3.20±0.07	4.05±0.11*	3.56±0.10$^{\#}$
LW/ BW (mg/g)	3.97±1.82	4.88±0.17*	4.22±0.11$^{\#}$
Infarct size (%)		42.3±3.36	34.3±2.09$^{\#}$

Data are presented as mean ± SEM (n = 8 per group). MI, myocardial infarction; BW, body weight; HW, heart weight; LW, lung weight.*, $p<0.05$, vs Sham, $^{\#}$, $p<0.05$, vs MI.

Figure legends

Figure 1 Effects of butyrate on MI-induced cardiac dysfunction and hemodynamic disorder. **(A-C)**, Echocardiographic measurements of LVEDD, EF and FS of Sham, MI and butyrate+ MI rats at 7 days after MI (n=8). **(D, E)**, Quantitative analysis of maximal rate of rise (dP/dtmax) and fall (dP/dtmin) of LV pressure (n=6). **(F)**, Quantification of serum BNP levels by ELISA analysis (n=4). Data shown as mean ± SEM; *$p < 0.05$, **$p < 0.01$. NS, no significant.

Figure 2 Effects of butyrate on electrical properties and ventricular tachyarrhythmia vulnerability of the hearts post-MI. Representative ECG episode *in vivo* **(A)** and quantitative analysis of ECG parameters including the P wave duration, PR intervals and QJ intervals at 7 days post-MI (n=8) **(B-D)**. Representative recordings of burst pacing in Langendorff-perfused hearts to induce ventricular tachycardia (VT+VF) **(E)**, and inducibility of VTA in three groups **(F)**. The number of hearts in each group is indicated in histogram. Data shown as mean ± SEM; *p < 0.05, **p < 0.01. NS, no significant.

Figure 3 Effects of butyrate on inflammatory responses following MI. **(A-F),** TNF-α, IL-1β and IL-10 mRNA and protein expression levels by RT-PCR and Elisa analysis in the infarct border zone (IBZ) at 3 days post-MI treated with butyrate. **(G)**, Representative images of LV sections by immunofluorescence staining, sections stained with anti-CD68 (red), anti-CD163 (green) antibodies, and DAPI (blue). Scale bar for 50 μm. **(H, I)**, the percentages of $CD68^+$ and $CD163^+/CD68^+$ macrophages are shown in the graph. **(J, K)**, RT-PCR assays of CD68 and CD163 in hearts. Data shown as mean ± SEM (n=4); *p < 0.05, **p < 0.01. NS, no significant.

Figure 4 Effects of butyrate on NGF and NE production following MI. **(A-C),** Representative immunofluorescence images and quantification showing the expression of CD68 (green), NGF (red), and DAPI (blue) staining in the IBZ LV sections subjected to MI operation for up to 3 day. Scale bar for 50 μm. **(D)**, Quantitative PCR analysis of NGF. **(E, F)**, Quantification of NE levels of plasma and cardiac tissue by ELISA analysis. Data shown as mean ± SEM (n=4); *p < 0.05, **p < 0.01.

Figure 5 Effects of butyrate on cardiac sympathetic hyperinnervation and nerve sprouting after MI. **(A)**, the staining profile of cardiac sympathetic hyperinnervation with TH and nerve sprouting with GAP43 antibody is shown in red, nuclei with DAPI are stained in blue. Scale bar for 50 μm. **(B, C)**, the percentages of TH and GAP43 in the IBZ of hearts at 7 days after MI are shown in the graph. **(D, E)**, Representative western bolts and quantification of TH and GAP43 expressions. Data shown as mean ± SEM (n=4); *p < 0.05, **p < 0.01.

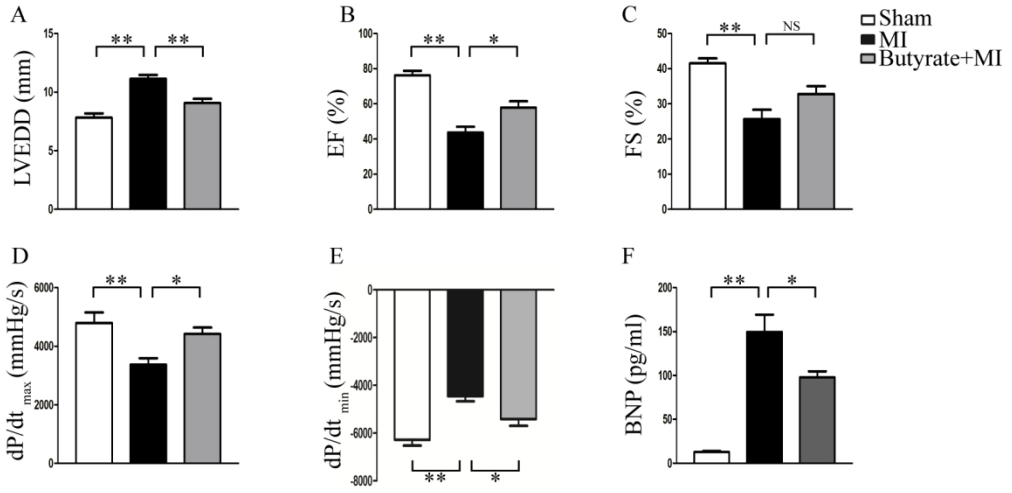

Figure 1 Effects of butyrate on MI-induced cardiac dysfunction and hemodynamic disorder.

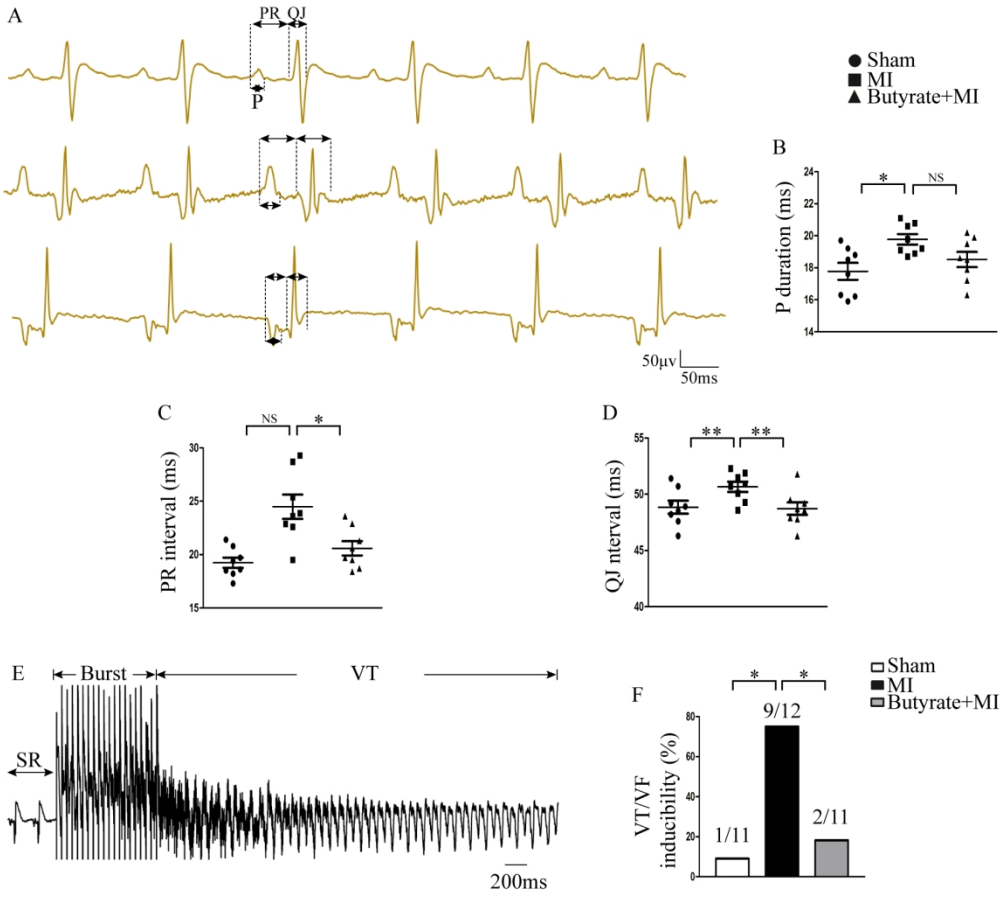

Figure 2 Effects of butyrate administrated MI rats on electrical properties and ventricular tachyarrhythmia vulnerability of the hearts.

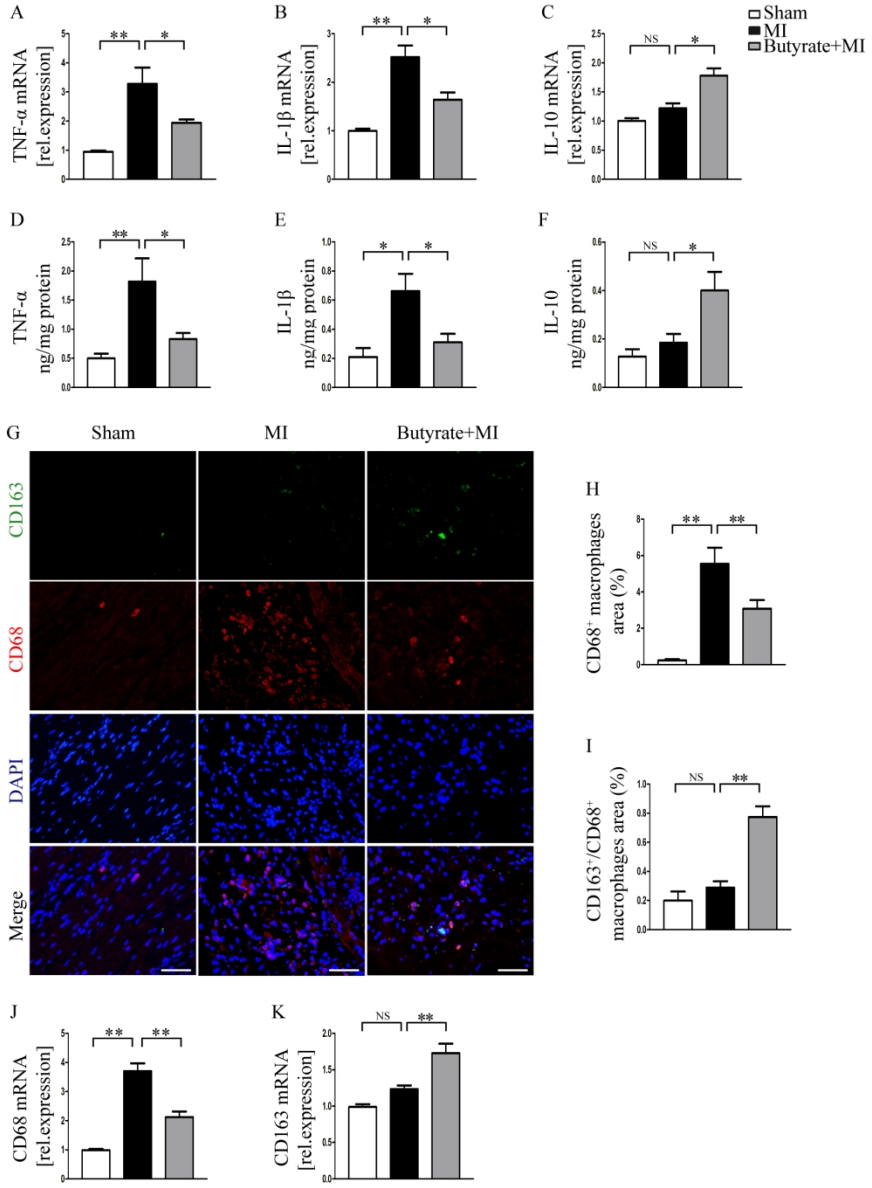

Figure 3 Effects of butyrate on inflammatory responses following MI.

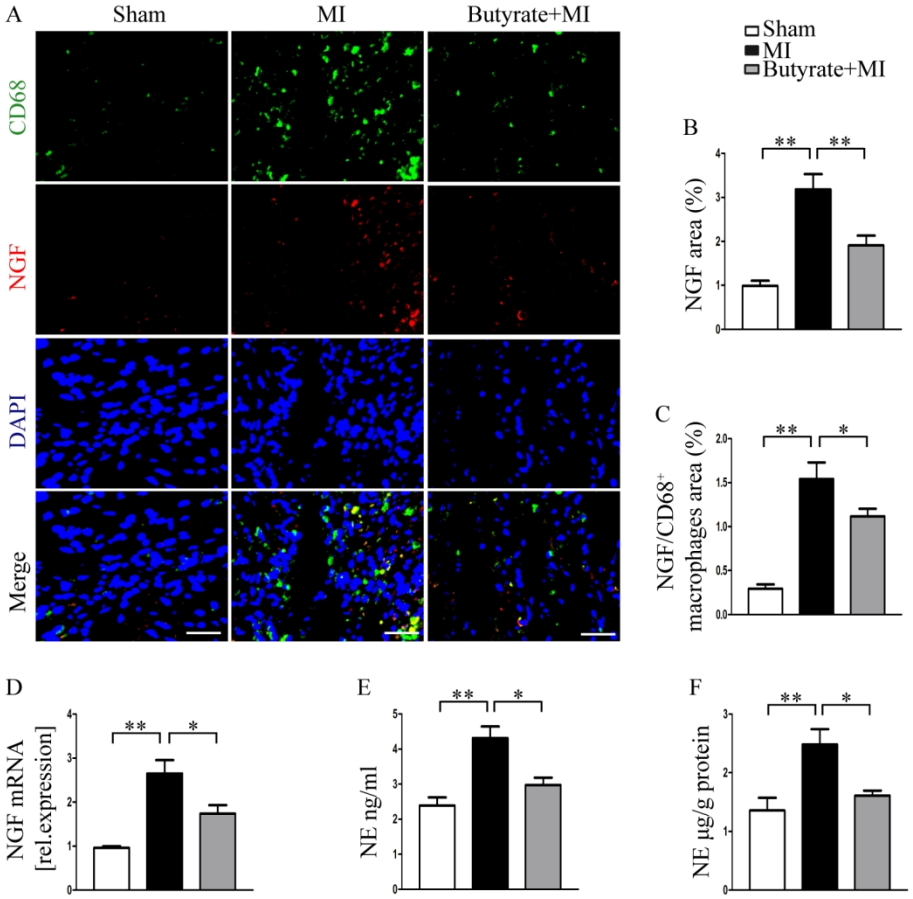

Figure 4 Effects of butyrate on NGF and NE production following MI.

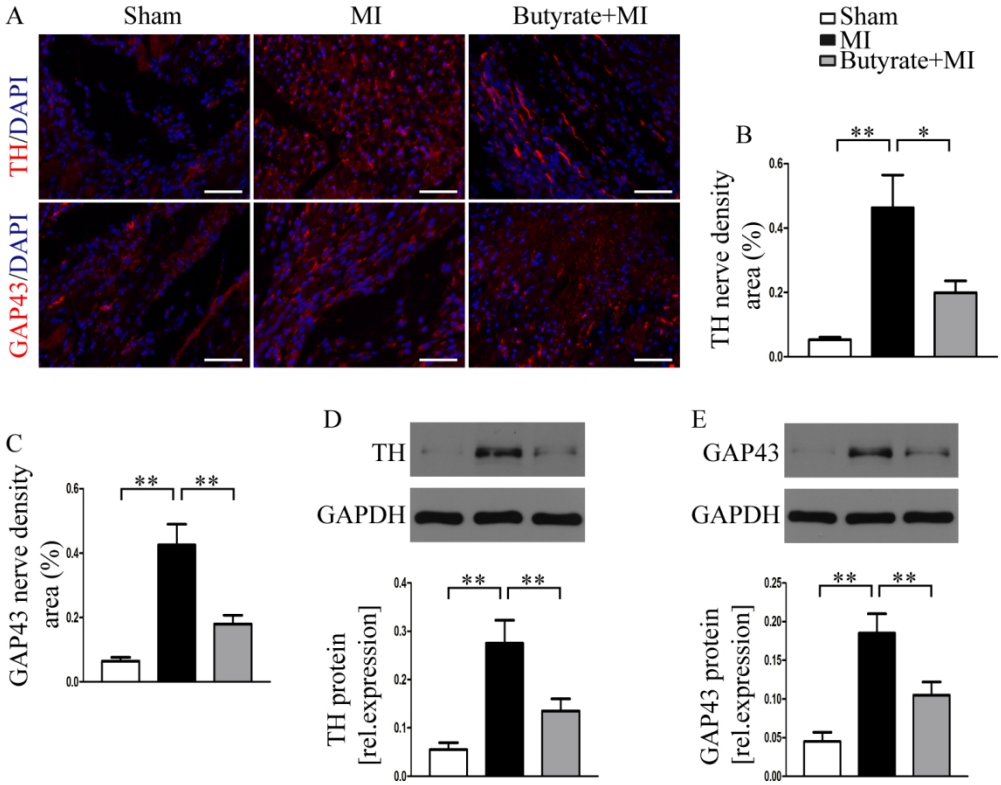

Figure 5 Effects of butyrate on cardiac sympathetic hyperinnervation and nerve sprouting after MI.